Available online at www.sciencedirect.com
SCIENCE DIRECT
Journal of Molecular Spectroscopy 237 (2006) 259– 270
Journal of MOLECULAR SPECTROSCOPY
www.elsevier.com/locate/jms

High resolution electronic study of $^{16}O^{14}N^{16}O$, $^{16}O^{14}N^{18}O$ and $^{18}O^{14}N^{18}O$: A rovibronic survey covering 11 800–14 380 cm^{-1}

E.A. Volkers [a], J. Bulthuis [a], S. Stolte [a], R. Jost [b], H. Linnartz [c,*]

[a] *Department of Physical Chemistry, Laser Centre Vrije Universiteit, De Boelelaan 1083, NL 1081 HV Amsterdam, The Netherlands*
[b] *Laboratoire de Spectrométrie Physique, Université Joseph Fourier de Grenoble, B.P. 87, F 38402 Saint Martin d'Hères Cedex, France*
[c] *Sackler Laboratory for Astrophysics, Leiden Observatory, Postbus 9513, NL 2300 RA Leiden, The Netherlands*

Received 22 February 2006; in revised form 27 March 2006
Available online 4 April 2006

Abstract

The 11 800–14 380 cm^{-1} frequency range has been scanned for rotationally resolved rovibronic transitions in the A^2B_2–X^2A_1 electronic band system of the symmetric (C_{2v}) $^{16}O^{14}N^{16}O$ and $^{18}O^{14}N^{18}O$ isotopologues and in the corresponding electronic band system of the asymmetric (C_s) $^{18}O^{14}N^{16}O$ isotopologue. The rotational analysis—reflecting minor differences in mass—in combination with symmetry induced spectral differences allows an identification of 68 $^{16}O^{14}N^{16}O$ vibronic levels, 26 $^{18}O^{14}N^{18}O$ vibronic levels and 51 $^{18}O^{14}N^{16}O$ vibronic levels. The bands are recorded using near infrared fluorescence spectroscopy and a piezo valve based pulsed molecular beam expansion of premixed $^{18}O_2$ and $^{14}N^{16}O$ in Ar. The majority of the observed bands is rotationally assigned and can be identified as transitions starting from the vibrational ground state of one of the isotopologues. Numerous hot bands have also been identified. A comparison of the overall spectroscopic features of C_{2v} vs. C_s symmetric species provides qualitative information on symmetry dependence of vibronic couplings.

Keywords: High resolution spectroscopy; Electronic spectroscopy; NO_2 isotopologues; Conical intersection; Symmetry considerations

1. Introduction

In recent years several spectroscopic studies have focused on the complexity of the A^2B_2–X^2A_1 electronic spectrum of nitrogen-dioxide, NO_2 [1–17]. This spectrum is very dense and vibronically highly irregular as a consequence of a strong vibronic coupling between the X^2A_1 ground state and the lowest electronically excited A^2B_2 state via the asymmetric stretch coordinate of b_2 symmetry. The interaction takes place above the conical intersection of the two potential energy surfaces at a rather low energy of about 10 000 cm^{-1} and as a consequence, spectral features have been vibronically assigned only well below and close to the conical intersection. For higher energies vibrational assignments are generally ambiguous because of significant vibronic couplings.

In the last decade studies have been reported that mainly focus on the main isotopologue; $^{16}O^{14}N^{16}O$. These comprise applications of a number of techniques, such as ICLAS [18], CRD [19], LIF [20] and bolometric detection [10,12]. For the other isotopologues optical information is largely lacking, mainly because of problems related to the high costs involved in studying ^{15}N- and ^{18}O-isotopes. For this reason we have recently constructed a spectroscopic setup in which large frequency domains are scanned automatically with high sensitivity and high spectral accuracy at a minimal gas consumption [21]. In this way more than 250 rotationally resolved vibrational bands of the A^2B_2–X^2A_1 electronic transition of the $^{16}O^{15}N^{16}O$ isotopologue have been observed in the 14 300–18 000 cm^{-1} range [1] and the present study is an extension of this work to the symmetric $^{18}O^{14}N^{18}O$ and asymmetric $^{16}O^{14}N^{18}O$ isotopologues in the 11 800–14 380 cm^{-1} range. This energy range covers roughly polyads 3–6 of the A^2B_2 state (see Fig. 2 of Ref. [15]). In addition, more accurate information

* Corresponding author. Fax: +31 71 5275819.
E-mail address: linnartz@strw.leidenuniv.nl (H. Linnartz).

0022-2852/$ - see front matter © 2006 Elsevier Inc. All rights reserved.
doi:10.1016/j.jms.2006.03.012

for the main isotopologue in this frequency domain has been obtained. The recorded rotational spectra reflect the differences in molecular masses, resulting in rotational constants with average values around 0.42, 0.40 and 0.38 cm^{-1} for $^{16}O^{14}N^{16}O$, $^{18}O^{14}N^{16}O$ and $^{18}O^{14}N^{18}O$, respectively. C_{2v} and C_s species yield clearly different spectra.

The present paper is organized in the following way. After a short overview of the experimental procedure, results are presented for the three isotopologues in their A^2B_2–X^2A_1 (A^2A'–X^2A') electronic band system.[1] The spectroscopic fitting procedure is shortly discussed and examples are shown to visualize typical spectra from which the spectroscopic constants are derived. The spectroscopic constants are summarized in three separate overview tables. The paper ends with a spectroscopic section in which differences that are due to symmetry properties are discussed.

2. Experiment

The experimental setup has been described in detail recently [21]. The second harmonic of a Nd:YAG laser is used to pump a tunable dye laser covering the energy range of 11 800–14 380 cm^{-1} using Styryl 9, 8 and 7 dyes with a typical bandwidth of 0.07 cm^{-1}. The laser beam is focused onto an expanding beam of a premixed 5% $^{18}O_2/^{14}N^{16}O$ (1:2) in Ar sample. Oxidation and isotope exchange reactions in the mixture result in the presence of both $^{16}O^{14}N^{16}O$, $^{18}O^{14}N^{16}O$ and $^{18}O^{14}N^{18}O$ species. This has been tested by recording a mass spectrum of sample gas that is discharged by electron impact ionization through a cw expansion and subsequently monitored by a quadrupole mass spectrometer a few centimeters downstream [22,23]. Strong mass peaks are found at the corresponding masses of 46, 48 and 50 amu. The small gas consumption is achieved by using a high intensity piezo electric pulsed molecular beam source that is optimized for a well-defined short pulse shape with an opening time of 150 μs. A LN_2 cooled Ge detector (North Coast EO-817L), sensitive in the 0.8–1.7 μm region, is used to monitor the fluorescence zone that is about 1.5 cm downstream of the nozzle orifice. Cut-off filters are used to shield the detector from residual laser light. Typically 10 laser shots are averaged for each data point for the stronger bands and up to 40 laser shots for the weaker ones. An absolute frequency calibration with an accuracy better than 0.05 cm^{-1} is obtained by simultaneously recording the output of a wavemeter. As the setup has been designed for fully automatic scanning over large frequency ranges an etalon signal with a FSR of 1.22 cm^{-1} is recorded to correct for non-linearities. An additional check of the absolute frequencies is also possible from band origin positions available for the main isotopologue in this frequency domain [18]. A comparison of the absolute band intensities in different frequency regimes is hard, mainly because of problems related to frequency dependent power variations of the dye laser. Within the band structure of one isotopologue, however, relative intensities are used to guide the rotational assignments.

3. Results and interpretation

The 11 800–14 380 cm^{-1} frequency region has been scanned at high resolution and this has resulted in the detection of 170 bands. The majority of these bands is assigned to rovibronic transitions originating from $^{16}O^{14}N^{16}O$ (80), $^{18}O^{14}N^{18}O$ (29) or $^{18}O^{14}N^{16}O$ (61) transitions, starting from the vibrational ground state or from vibrationally excited (hot band) levels. Band origin positions have been published before for the main isotopologue [11,18] but accurate fits are lacking. Resolved rovibronic data are not available for the other two isotopologues. So far only pure rotational and rovibrational studies have been performed that provide accurate ground state rotational constants for the majority of isotopic combinations [24–29]. These constants are summarized in Table 1. In Figs. 1–3 rotationally resolved spectra are presented for typical bands of $^{16}O^{14}N^{16}O$, $^{18}O^{14}N^{18}O$ and $^{18}O^{14}N^{16}O$, respectively, in the A^2B_2–X^2A_1 electronic system. The corresponding line positions are given in Tables 2, 4 and 6, respectively. The number of rotational transitions per band is limited because of the low rotational temperature (~10 K). The vibrational temperature is much higher and results in the appearance of a number of hot bands. These start mainly from the excited bending state $(v_1, v_2, v_3) = (0, 1, 0)$. The rotational and vibrational values used for these bands are listed in Table 1 as well. These hot bands (indicated by HB in the overview Tables 3, 5 and 7) are easily identified by determining differences in band origin positions and comparing excited state rotational and fine structure constants that must be identical for hot band and corresponding cold band (CB). From the figures it becomes clear that there exists a clear difference in spectral appearance between C_{2v} (Figs. 1 and 2) and C_s (Fig. 3) species. For symmetric isotopologues only even (odd) rotational quantum numbers are allowed in the $K = 0$ stack of A_1 (B_2) vibronic symmetry. In the asymmetric case no symmetry limitation exists and all subsequent transitions are observed, resulting in regular series of P- and R-branch transitions, independent of the K-value. For $K = 1$ states transitions starting from all levels are observed as well as Q-branch transitions. These $K = 1$ transitions can be hard to identify because they are significantly weaker and less regular (larger spin-splittings) than $K = 0$ sub-bands. This is due to the cooling in the expansion and because the intensity is spread over a larger number of allowed transitions. In addition, it happens that a $K = 1$ sub-band shifts outside its corresponding $K = 0$ sub-band and consequently will be hard to recognize. In the case of $^{15}NO_2$ [1] about 30 $K = 1$ sub-bands on a total of 250 bands were identified. In the present case substantially less and mainly $^{16}O^{14}N^{16}O$ transitions are unambigu-

[1] Throughout this whole paper the diabatic labeling A^2B_2–X^2A_1 is used.

Table 1
Overview of the ground (0,0,0) and $(0,v_2,0)$ and $(v_1,0,0)$ excited rovibrational constants (cm^{-1}) for different $^{x}O^{y}N^{z}O$ isotopologues used or derived in this work

	v_{bo}	A''	B''	C''	ε''_{11}	ε''_{22}	ε''_{33}	Ref.
$^{16}O^{14}N^{16}O$								
(0,0,0)	0	8.0024	0.4337	0.4105	0.1803	0.0003	−0.0032	[24]
(0,1,0)	749.65	8.3741	0.4336	0.4096	0.1986	0.0002	−0.0032	[25]
(1,0,0)	1319.77	8.0933	0.4313	0.4093	0.1834	0.0002	−0.0033	[26]
$^{18}O^{14}N^{18}O$								
(0,0,0)	0	7.7217	0.3855	0.3664	—	—	—	[29]
(0,1,0)	722.9	8.0543	0.3854	0.3657	—	—	—	[29]
$^{18}O^{14}N^{16}O$								
(0,0,0)	0	7.8656	0.4091	0.3880	0.1777	0.0003	−0.0030	[27]
(0,1,0)	736.4	—	0.409	0.388	—	—	—	This work

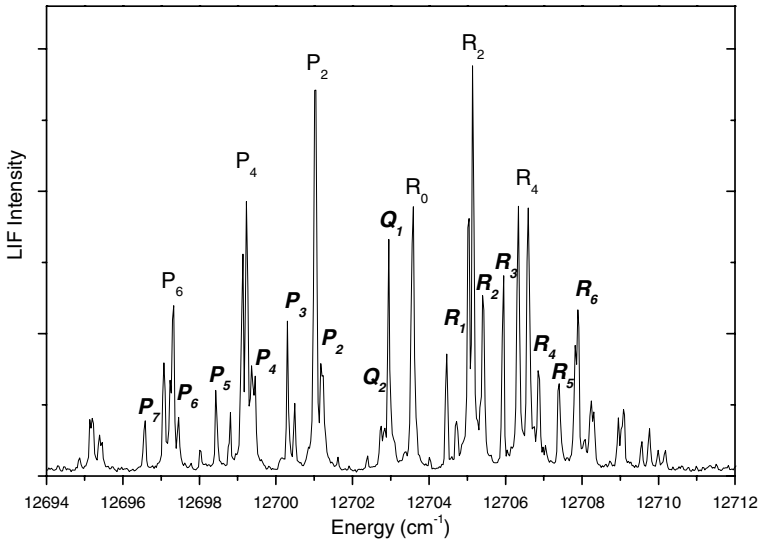

Fig. 1. An example of a typical band within the A^2B_2–X^2A_1 electronic system of $^{16}O^{14}N^{16}O$ consisting of $K=0$ and $K=1$ sub-bands, both with resolved fine structure. For $K=0$ only transitions starting from even N-levels are observed, for $K=1$ transitions both odd and even N-levels are involved. In addition, a Q-branch becomes visible. The line positions with assignment are listed in Table 2 and the resulting constants are available from Table 3 (CB14).

ously identified as originating from $K=1$. For the other two isotopologues, particularly $^{18}O^{14}N^{16}O$, only Q-branches have been observed for $K=1$. It is clear that a larger set of $K=1$ bands is expected, but under the present experimental conditions, a substantial number of $K=1$ transitions is definitely not observed. Finally, also fine structure splittings are observed, mainly for the $^{16}O^{14}N^{16}O$ isotopologue, whereas for $^{18}O^{14}N^{16}O$ and also $^{18}O^{14}N^{18}O$ the number of bands with resolvable splittings is substantially smaller.

In the three overview tables the spectroscopic constants are summarized for all identified bands. The center frequencies that are used in the fits are determined by fitting individual transitions by a Gaussian function. To account for the full rotational spectrum the Hamiltonian should consist of terms describing the rigid rotor part, the fine structure interaction and distortional effects: $H = H_{rigid} + H_{fs} + H_{cf}$. This has been explained in detail in Ref. [1] and is repeated here for clarity.

Since NO_2 is a nearly symmetric top, energy levels are described by

$$E = v_{bo} + \frac{B+C}{2}N(N+1) + \left(A - \frac{B+C}{2}\right) \times \left(K^2 + C_1\left(\frac{C-B}{2A-B-C}\right) + C_2\left(\frac{C-B}{2A-B-C}\right)^2 + C_3\left(\frac{C-B}{2A-B-C}\right)^3\right), \quad (1)$$

where v_{bo} indicates the band origin, A, B and C are rotational constants, N is the rotational quantum number, K is the projection of N on the molecular a-axis and C_1, C_2 and C_3 are constants defined in Appendix III of Ref. [30]. Note that the asymmetric top contributions C_1, C_2 and C_3 are zero for $K=0$. Accurate rotational constants are available for the ground state (0,0,0) from experiment for $^{16}O^{14}N^{16}O$ and $^{18}O^{14}N^{16}O$ and from theory for $^{18}O^{14}N^{18}O$. The hot band constants have been measured

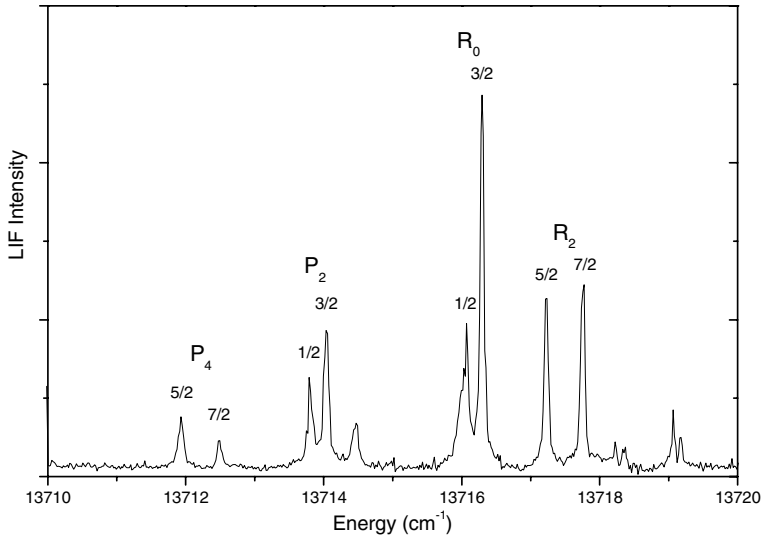

Fig. 2. An example of a typical band within the A^2B_2–X^2A_1 electronic system of $^{18}O^{14}N^{18}O$ consisting of a $K = 0$ sub-band with resolved fine structure. The line positions with assignment are listed in Table 4 and the resulting constants are available from Table 5 (CB16).

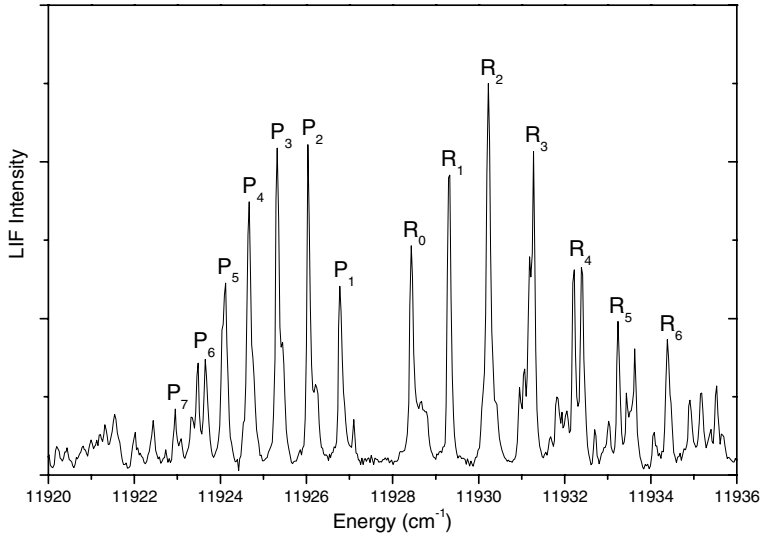

Fig. 3. An example of a fully resolved rovibronic transition of $^{18}O^{14}N^{16}O$ consisting of a $K = 0$ sub-band with observable fine structure for higher N-values. In the asymmetric species (C_s symmetry) transitions starting from odd and even N-levels are observed. The line positions with assignment are listed in Table 6 and the resulting constants are available from Table 7 (CB3). Although no $K = 1$ transitions have been analyzed for this isotopologue, Q-branches of $K = 1$ sub-bands are visible as can be seen from this figure.

for $^{16}O^{14}N^{16}O$ and calculated for $^{18}O^{14}N^{18}O$, whereas for $^{18}O^{14}N^{16}O$ only estimates are available. All values with corresponding references are summarized in Table 1.

In the fit program the series expansion is carried to the third order. This is more than sufficient for the experimental accuracy of the line positions in our measurements. In a limited number of cases also fine structure is resolved and the observed splittings are fitted—independently for $K = 0$ and $K = 1$ sub-bands—using an expression for the spin-rotation energy of an asymmetric top molecule given by

$$E_{SR} = \frac{1}{2}\varepsilon_N[J(J+1) - N(N+1) - S(S+1)], \quad (2)$$

where, for a molecule with C_{2v} symmetry, ε_N can be written in terms of diagonal tensor elements only

$$\varepsilon_N = \frac{1}{2}(\varepsilon_{bb} + \varepsilon_{cc}) + \frac{\varepsilon_{aa} - \frac{1}{2}(\varepsilon_{bb} + \varepsilon_{cc})}{N(N+1)}K^2 \pm \frac{1}{4}\delta_{|K|,1}(\varepsilon_{bb} - \varepsilon_{cc}). \quad (3)$$

The + and − sign corresponds to the symmetric and anti-symmetric Wang combination of symmetric top functions, respectively. For $|K| = 1$, $\delta_{|K|,1}$ is unity and zero otherwise. Each rotational level splits into two levels, with $J = N + 1/2$ and $J = N - 1/2$, leading to respective energy shifts of $1/2N\varepsilon_N$ and $-1/2(N+1)\varepsilon_N$. For the electronic and

Table 2
Observed and calculated line positions (cm^{-1}) for both $K=0$ and $K=1$ sub-bands of the band at 12703 cm^{-1} (CB 14—Table 3) in the A^2B_2–X^2A_1 electronic system of $^{16}O^{14}N^{16}O$ as shown in Fig. 1

		ν_{obs}	ν_{calc}	Obs. − calc.
$K=0$				
P_6	(9/2)	12697.07	12697.08	−0.01
P_6	(11/2)	12697.31	12697.31	0.00
P_4	(5/2)	12699.12	12699.10	0.02
P_4	(7/2)	12699.24	12699.24	−0.00
P_2	(1/2)	12701.03	12701.01	0.02
P_2	(3/2)	12701.03	12701.06	−0.04
R_0	(1/2)	12703.58	12703.54	0.04
R_0	(3/2)	12703.58	12703.59	−0.02
R_2	(5/2)	12705.03	12705.01	0.02
R_2	(7/2)	12705.15	12705.15	0.00
R_4	(9/2)	12706.33	12706.37	−0.04
R_4	(11/2)	12706.60	12706.59	0.00
$K=1$				
P_7	(13/2)	12696.57	12696.53	0.04
P_7	(11/2)	12696.57	12696.55	0.02
P_6	(9/2)	12697.23	12697.19	0.04
P_6	(11/2)	12697.45	12697.43	0.01
P_5	(9/2)	12698.44	12698.48	−0.05
P_4	(5/2)	12699.37	12699.27	0.10
P_4	(7/2)	12699.37	12699.39	−0.02
P_3	(5/2)	12700.30	12700.36	−0.06
P_3	(3/2)	12700.49	12700.43	0.06
P_2	(3/2)	12701.20	12701.22	−0.02
Q_2	(5/2)	12702.74	12702.77	−0.03
Q_2	(3/2)	12702.84	12702.88	−0.04
Q_1	(3/2)	12702.95	12702.94	0.01
Q_1	(1/2)	12702.95	12703.04	−0.10
R_1	(5/2)	12704.46	12704.49	−0.03
R_1	(3/2)	12704.72	12704.66	0.07
R_2	(7/2)	12705.41	12705.37	0.05
R_3	(9/2)	12705.94	12705.97	−0.03
R_3	(7/2)	12705.94	12706.03	−0.09
R_4	(11/2)	12706.87	12706.84	0.03
R_5	(13/2)	12707.40	12707.34	0.06
R_5	(11/2)	12707.40	12707.38	0.02
R_6	(13/2)	12707.87	12707.90	−0.02
R_6	(15/2)	12708.24	12708.24	−0.00

vibrational ground state, the fine structure coupling is relatively small as can be seen from Table 1. In the fit program we have used the listed values as taken from Ref. [24] for $^{16}O^{14}N^{16}O$ and from Ref. [27] for $^{18}O^{14}N^{16}O$. For $^{18}O^{14}N^{18}O$ experimental values are unavailable, but as $K=1$ bands have not been observed for this specific isotopologue and as for $K=0$ sub-bands only $\varepsilon_N = \frac{1}{2}(\varepsilon_{bb}+\varepsilon_{cc})$ counts, this does not matter. From the fitted excited state ε' values listed in the overview tables, it becomes clear that both magnitude and sign vary greatly between different vibronic states. This variability is the very consequence of (ro)vibronic interactions, since the ε' values depend strongly on the degree of mixing of the coupled states.

The centrifugal distortion part of the Hamiltonian is written as

$$H_{cf} = D_N N^2 (N+1)^2. \quad (4)$$

On the basis of experimental data [31] D_N is expected to be of the order of 10^{-4} cm^{-1}. At the low final rotational temperature in the beam only a few low lying levels are populated and including Eq. (4) into the fit only makes sense in those (few) cases where several levels ($N>5$) are observed.

In the next three paragraphs spectra recorded for the individual isotopologues are discussed in detail. Only bands with acceptable S/N are taken into account. Weak bands, for which only a few transitions are observed and accurate fits are not possible, are not listed.

3.1. $^{16}O^{14}N^{16}O$

A typical example of a rotationally resolved rovibronic band of symmetric $^{16}O^{14}N^{16}O$ in its X^2A_1–A^2B_2 electronic system is shown in Fig. 1. The band appearance represents the most complicated case in which both $K=0$ and $K=1$ bands and also fine structure splitting is observed. The

Table 3
Overview of the excited state molecular parameters (cm^{-1}) of all identified rovibronic bands observed in the A^2B_2–X^2A_1 electronic system of $^{16}O^{14}N^{16}O$ in the 11 800–14 380 cm^{-1} range

		Origin	Origin [11,18]	Origin cold band	$1/2(B'+C')$	Centrif. dist. const.	$1/2(\varepsilon'_{22}+\varepsilon'_{33})$	$\Delta(1/2\,(B'+C'))\times10^3$	Ground level
(a) $K=0$									
CB	1	11807.80	11807.80		0.420		0	0.5	
CB	2	11847.81	11847.75		0.400		0.048	0.6	
CB	3	11960.75	11960.70		0.431		−0.154	0.5	
CB	4	12059.15	12059.01		0.422		−0.094	0.6	
CB	5	12100.90	12100.90		0.427	0.0000	0	1.0	
CB	6	12177.09	12177.06		0.443		0	0.5	
CB	7	12263.35	12263.28		0.416	0.0000	0	1.0	
CB	8	12340.33	12340.52		0.449	0.0003	0	0.5	
CB	9	12410.76	12410.71		0.418		−0.018	0.6	
CB	10	12446.08	12446.03		0.434		0.015	0.6	
CB	11	12575.86	12575.57		0.425		−0.507	0.9	
CB	12	12600.28	12600.44		0.437		0.406	0.6	
CB	13	12668.15	12668.13		0.411	0.0001	0	1.0	
CB	14	12702.77	12702.62		0.405		0.036	0.5	
CB	15	12723.97	12723.87		0.426	0.0002	−0.095	1.0	
CB	16	12739.83	12739.83		0.419		0	0.5	
HB	35	12761.30	12761.27	13510.98	0.427		0.101	0.6	(0,1,0)
CB	17	12863.13	12863.18		0.426		0	0.6	
CB	18	12916.29	12916.29		0.411	0.0000	0	1.2	
CB	19	12985.74	12985.84		0.375		−0.216	1.7	
CB	20	13008.71	13008.84		0.426		−0.074	0.6	
CB	21	13020.64	13020.74		0.415		0	1.4	
CB	22	13047.43	13047.51		0.399		0	1.7	
HB	48	13061.10	13061.19	13810.89	0.416		0	1.4	(0,1,0)
HB	49	13081.53	13081.44	13831.17	0.414		0.065	1.8	(0,1,0)
CB	23	13088.33	13088.36		0.418		0.004	1.6	
CB	24	13158.39	13158.32		0.411		0.003	0.6	
CB	25	13184.61	13184.57		0.424		0.010	0.6	
CB	26	13208.62	13208.59		0.417		−0.126	0.6	
HB	53	13213.83		13963.47	0.424		−0.021	1.7	(0,1,0)
CB	27	13222.93	13222.89		0.421		0.015	0.7	
HB	54	13234.87	13234.89	13984.52	0.421		0	1.4	(0,1,0)
CB	28	13264.27	13264.33		0.402		0	0.6	
HB	57	13272.43	13272.71	14022.28	0.412		−0.241	0.6	(0,1,0)
CB	29	13285.14	13285.22		0.425		0.042	0.6	
HB	58	13320.81	13320.91	14070.56	0.402		0.069	0.6	(0,1,0)
CB	30	13352.76	13352.68		0.404		0	1.7	
HB	60	13379.11	13379.04	14128.72	0.414		−0.097	0.9	(0,1,0)
CB	31	13395.63	13395.71		0.480		−0.248	1.4	
CB	32	13406.21	13406.18		0.452		−0.031	0.6	
HB	62	13422.68		14172.26	0.401		0.418	2.9	(0,1,0)
CB	33	13426.58	13426.58		0.402		0	0.6	
HB	63	13427.89	13427.82	14177.47	0.458		0	1.4	(0,1,0)
HB	64	13465.41	13465.40	14215.02	0.416		0.026	1.7	(0,1,0)
CB	34	13477.11	13477.04		0.417		0	0.6	

CB	35	13510.98	13510.92		0.427		0.100	0.6		
CB	36	13552.81	13552.80		0.406		−0.013	0.6		
CB	37	13576.79	13576.76		0.428		−0.175	1.7		
CB	38	13591.48	13591.40		0.403		0.076	0.6		
HB		13614.61	13614.57	14934.20	0.423		0	1.7	(1,0,0)	
CB	39	13621.70	13621.90		0.513		0.186	1.7		
CB	40	13641.60	13641.58		0.419		0	1.7		
CB	41	13680.33	13680.30		0.418		0.026	1.6		
CB	42	13730.80	13730.70		0.413		0	1.7		
CB	43	13742.20	13742.14		0.390		−0.113	1.4		
CB	44	13766.89	13766.68		0.365		−0.130	1.4		
CB	45	13783.53	13783.50		0.403		0	0.6		
CB	46	13791.29	13791.25		0.430		−0.029	0.7		
CB	47	13810.89	13810.84		0.414		−0.032	0.6		
CB	48	13831.17	13831.16		0.416		0.061	1.4		
CB	49	13858.39	13858.38		0.427		0.042	1.7		
CB	50	13932.23	13932.33		0.424		0	1.4		
CB	51	13954.22	13954.17		0.404		0	0.6		
CB	52	13963.47	13963.47		0.422		−0.029	0.9		
CB	53	13984.52	13984.54		0.417		0	0.6		
CB	54	13993.92	13993.96		0.418		0.042	0.7		
CB	55	14003.25	14003.27		0.424		0	0.6		
CB	56	14022.28	14022.36		0.396		−0.285	1.4		
CB	57	14070.56	14070.56		0.400		0.080	1.0		
CB	58	14098.67			0.428		0	0.6		
CB	59	14128.72	14128.73		0.416	0.0001	−0.088	1.2		
CB	60	14137.74	14137.93		0.569	0.0012	−0.148	1.1		
CB	61	14172.26	14172.22		0.398		0.426	1.6		
CB	62	14177.47	14177.53		0.452		0	0.6		
CB	63	14215.02	14215.05		0.416		0.021	1.4		
CB	64	14254.04	14254.08		0.425		0	0.6		
CB	65	14286.25	14286.10		0.362		−0.056	0.9		
CB	66	14310.86	14310.87		0.422		0	1.4		
CB	67	14317.35	14317.38		0.413		0	0.6		
CB	68	14346.01	14345.99		0.408		−0.065	0.6		

		Origin	A'	B'	C'	Centrif. dist. const.	$\varepsilon'_{K=0}$	ε'_{11}	ε'_{22}	ε'_{33}	$\Delta(1/2(B'+C'))\times 10^3$
(b) $K=1$											
CB	5	12100.90	11.591	0.457	0.396	0.0000	−0.006	0.141	0.003	0.004	0.9
CB	8	12340.41	15.580	0.440	0.433	0.0001	−0.005	0.194	0.001	−0.001	1.0
CB	9	12410.75	9.683	0.430	0.407	0.0000	−0.018	0.281	−0.009	−0.010	2.2
CB	10	12446.11	12.964	0.516	0.341	−0.0003	0.014	0.168	0.000	0.000	2.2
CB	14	12702.77	8.203	0.413	0.394	−0.0001	0.036	−0.036	−0.027	0.076	1.2
CB	15	12723.98	8.422	0.443	0.405	0.0002	−0.095	0.025	−0.004	0.046	0.9

HB# indicates a hot band that corresponds to a cold band CB#.

assignment is indicated in the figure. For $K = 0$ only even N-levels are symmetry allowed and as a consequence the $K = 0$ sub-band consists of $P_{2,4,6}$ and $R_{0,2,4,6}$ transitions. Q-branch transitions are not allowed in $K = 0$ but become visible in the $K = 1$ sub-band. In this $K = 1$ sub-band also N-transitions starting from odd levels become possible, which can be clearly observed from Fig. 1; the number of transitions in the $K = 1$ sub-band is about twice the number found for $K = 0$. For 'pure' $K = 0$ bands, only an effective rotational constant $\overline{B}' = 1/2(B' + C')$ can be derived. In the case of a resolved $K = 1$ band also the A' constant and independent values for B' and C' are determined. For the band shown in Fig. 1 all line positions are listed in Table 2. The frequencies are fitted following the procedure described in the previous paragraph and this yields values for the band origin $\nu_{bo} = 12702.77\ cm^{-1}$, the rotational constants $A' = 8.20\ cm^{-1}$, $B' = 0.413\ cm^{-1}$ and $C' = 0.394\ cm^{-1}$ and the fine structure constants $\varepsilon'_{K=0} = 0.036$, $\varepsilon'_{aa} = -0.036\ cm^{-1}$, $\varepsilon'_{bb} = -0.027\ cm^{-1}$ and $\varepsilon'_{cc} = 0.076\ cm^{-1}$. These values are in reasonable agreement with those reported in Ref. [11]. Note that the fine structure constants determined for the $K = 0$ and $K = 1$ sub-bands often slightly differ. This is due to the numerous rovibronic interactions which affect differently the various K manifolds as observed and analyzed for the $^{16}O^{14}N^{16}O$ isotopologue [17]. The resulting (obs. − calc.) values that are listed in Table 2, are typically of the order of $0.05\ cm^{-1}$ which is smaller than the linewidth of the laser system.

In total 80 bands are identified as originating from $^{16}O^{14}N^{16}O$ and in six cases an unambiguous identification of $K = 1$ sub-bands has been possible. In most cases a fine structure splitting is resolved. In total 11 bands can be assigned as originating from a hot band (0,1,0). For this isotopologue it is possible to label all observed bands with CB or HB as transitions in the range above $14380\ cm^{-1}$ are available from Ref. [20]. The averaged ν_2 value that follows from these differences amounts to $749.67(8)\ cm^{-1}$, which is in perfect agreement with the value listed in Table 1. The results are summarized in Table 3a for $K = 0$ and in Table 3b for $K = 1$. All these bands except one (CB58) have been reported in previous studies [11,20]. Note that the rotational and spin constants should only be considered as effective values describing the low lying rotational components ($N = 1$, 3, 5). In fact, rovibronic interactions perturb randomly the levels as mentioned and discussed previously [20]. The differences that exist between results listed in Table 3 of this paper and Table I of Ref. [11] are mostly due to the presence of local rovibronic perturbations which may or may not have been detected.

3.2. $^{18}O^{14}N^{18}O$

In Fig. 2 a rotationally resolved rovibronic band of the symmetric $^{18}O^{14}N^{18}O$ in its X^2A_1–A^2B_2 electronic system is shown. The spectroscopic behaviour is expected to be identical to that observed previously for symmetric $^{x}O^{y}N^{x}O$ species with the exception that for $^{18}O^{14}N^{18}O$ the ground state rotational constant ($\overline{B}'' = 0.38\ cm^{-1}$) amounts to about 90% of that determined for $^{16}O^{14}N^{16}O$ and $^{16}O^{15}N^{16}O$ ($\overline{B}'' = 0.42\ cm^{-1}$)—see Table 1. As a consequence the smaller rotational spacings allow a clear distinction between bands originating from the main isotopologue and $^{18}O^{14}N^{18}O$.

In total 28 bands have been observed; the majority has a 'pure' $K = 0$ sub-band appearance, with one exception for which a weak $K = 1$ band can be assigned (not listed in the table). Two bands are assigned as originating from a hot band (0,1,0) and only a few bands exhibit resolvable fine structure splitting. The line positions of the band shown in Fig. 2 are listed in Table 4 and (obs. − calc.) values are determined from a fitting procedure as described before. The fit yields $\nu_{bo} = 13715.51\ cm^{-1}$, an effective rotational constant $\overline{B}' = 0.356\ cm^{-1}$ and a fine structure constant of $\overline{\varepsilon}' = 0.153\ cm^{-1}$. A summary of the results obtained for all $^{18}O^{14}N^{18}O$ bands is given in Table 5.

Two of the 12 bands labeled #16 to 27 in Table 5 are assigned as cold band, but for the remaining bands this is not possible because of lacking spectral data above $14380\ cm^{-1}$. Using the ratio of the number of hot and cold bands observed in the main isotopologue (see Table 3a), we statistically expect only one hot band among these unlabelled bands. Two bands (HB19 and HB23) (in the range of the 1–15 CB series) are unambiguously identified as a hot band and this allows an accurate experimental determination of ν_2 ($^{18}O^{14}N^{18}O$) $= 722.3(3)\ cm^{-1}$. This is very close to the values of 722.8 and $722.9\ cm^{-1}$ given in Refs. [28,29].

3.3. $^{18}O^{14}N^{16}O$

A typical spectrum for the asymmetric $^{18}O^{14}N^{16}O$ is shown in Fig. 3. Because of the symmetry loss ($C_{2v} \rightarrow C_s$) all energy levels in $K = 0$ are allowed now and as a consequence regular, i.e., subsequent P- and R-branch transitions are observed. The line positions are listed in Table 6. A fit results in a band origin of $11927.58\ cm^{-1}$ and rotational parameters $A' = 8.89\ cm^{-1}$ and $1/2(B' + C') = 0.425\ cm^{-1}$. Obs. − calc. values are listed as well. In total 61 bands have been observed that can be

Table 4
Observed and calculated line positions (cm^{-1}) for the $K = 0$ band identified at $13715\ cm^{-1}$ (CB16—Table 5) in the A^2B_2–X^2A_1 electronic system of $^{18}O^{14}N^{18}O$ as shown in Fig. 2

	ν_{obs}	ν_{calc}	Obs. − calc.
$K = 0$			
P_4 (5/2)	13711.93	13711.95	−0.02
P_4 (7/2)	13712.49	13712.49	−0.00
P_2 (1/2)	13713.81	13713.81	−0.00
P_2 (3/2)	13714.04	13714.04	−0.00
R_0 (1/2)	13716.07	13716.06	0.00
R_0 (3/2)	13716.30	13716.29	0.00
R_2 (5/2)	13717.23	13717.21	0.02
R_2 (7/2)	13717.76	13717.75	0.00

Table 5
List with excited state molecular parameters (cm^{-1}) of rovibronic bands observed in the A^2B_2–X^2A_1 electronic system of $^{18}O^{14}N^{18}O$ in the 11800–14380 cm^{-1} range

		Origin	Origin cold band	$1/2(B'+C')$	Centrif. dist. const.	$1/2(\varepsilon'_{22}+\varepsilon'_{33})$	$\Delta(1/2(B'+C'))\times10^3$	Ground level
CB	1	11821.38		0.401	0.0001	0	1.0	
CB	2	12124.57		0.371	0.0000	0	1.0	
CB	3	12289.01		0.381		0	0.6	
CB	4	12328.76		0.372		0	1.4	
CB	5	12360.61		0.357		0	0.6	
CB	6	12520.37		0.396		0.053	0.5	
CB	7	12685.85		0.366		0	0.6	
CB	8	12990.14		0.363		−0.067	1.8	
HB	19	13065.76	13787.84	0.381		0	1.7	(0,1,0)
CB	9	13135.41		0.388		−0.063	0.7	
CB	10	13166.73		0.378		0	1.4	
HB	23	13187.28	13909.88	0.394		0	0.6	(0,1,0)
CB	11	13234.63		0.363		0	0.6	
CB	12	13249.79		0.372		0.062	1.4	
CB	13	13482.77		0.368		−0.129	0.7	
CB	14	13541.44		0.371		0	1.7	
CB	15	13659.99		0.357		0	1.7	
	16	13715.51		0.356		0.153	1.4	
	17	13735.94		0.425		−0.002	1.7	
	18	13766.75		0.390		0.054	1.8	
CB	19	13787.84		0.376		0	0.6	
	20	13800.34		0.383		0	1.7	
	21	13822.15		0.363		0	1.4	
	22	13868.06		0.377		0	0.6	
CB	23	13909.88		0.394		0	0.6	
	24	14023.29		0.368		0	1.7	
	25	14066.01		0.354		0	1.4	
	26	14189.97		0.366		0	1.4	
	27	14366.64		0.342		0.170	1.4	

HB# indicates a hot band that corresponds to a cold band CB#.

Table 6
Observed and calculated line positions (cm^{-1}) for the $K=0$ band identified at 11928 cm^{-1} (CB3—Table 7) for the asymmetric $^{18}O^{14}N^{16}O$ isotopologue as shown in Fig. 3

	ν_{obs}	ν_{calc}	Obs. − calc.
$K=0$			
P_7	11922.95	11922.96	−0.01
P_6 (9/2)	11923.47	11923.50	−0.03
P_6 (11/2)	11923.66	11923.52	0.14
P_5	11924.10	11924.08	0.01
P_4	11924.67	11924.69	−0.02
P_3	11925.33	11925.34	−0.01
P_2	11926.05	11926.04	0.01
P_1	11926.79	11926.78	0.01
R_0	11928.44	11928.43	0.02
R_1	11929.32	11929.33	−0.01
R_2	11930.23	11930.27	−0.04
R_3	11931.28	11931.26	0.02
R_4 (9/2)	11932.21	11932.27	−0.05
R_4 (11/2)	11932.40	11932.29	0.12
R_5	11933.25	11933.32	−0.07
R_6	11934.40	11934.38	0.03
$K=1$			
Q_1	11928.66	11928.66	0.00

assigned unambiguously to the asymmetric $^{18}O^{14}N^{16}O$. There are eight hot bands starting from (0,1,0) below 13600 cm^{-1}. This allows for a first time to determine experimentally a value for the ν_2 vibration: 736.36(12) cm^{-1}. The rotational parameters in the electronic ground state for these bands are estimated from the (0,0,0) values as available from [27]. Above 13,640 cm^{-1}, among the 23 observed bands, seven bands are cold bands because the

Table 7
List of excited state molecular parameters [cm^{-1}] of rovibronic bands observed for the asymmetric $^{18}O^{14}N^{16}O$ species in the 11 800–14 380 cm^{-1} range

		Origin	Origin cold band	A'	$1/2(B'+C')$	Centrif. dist. const.	$1/2(\varepsilon'_{22}+\varepsilon'_{33})$	$\Delta(1/2(B'+C'))\times10^3$	Ground level
CB	1	11831.78			0.415		0	0.9	
CB	2	11853.52		9.03	0.396	0.0000	0	1.1	
HB	14	11892.47	12628.63		0.44	0.0000	0	1.3	(0,1,0)
CB	3	11927.58		8.89	0.425	0.0001	0	0.8	
CB	4	11959.91		8.68	0.439		0	3.5	
CB	5	11985.37			0.409		0	0.5	
CB	6	12047.61		7.87	0.394	−0.0001	0	1.0	
CB	7	12213.51		7.12	0.422	0.0001	0	0.8	
CB	8	12270.71		7.36	0.413		0	0.6	
CB	9	12305.53		11.10	0.390	0.0000	0	1.1	
CB	10	12435.22		7.29	0.414		0	0.5	
CB	11	12470.40		8.01	0.421	0.0000	0	0.8	
CB	12	12510.72		9.89	0.387	0.0000	0	0.8	
CB	13	12532.78			0.408	−0.0001	0	0.9	
CB	14	12628.63		8.44	0.445	0.0001	0	0.4	
CB	15	12883.19			0.408	0.0000	0	1.1	
HB	32	12930.57	13667.04		0.39	0.0000	0	1.2	(0,1,0)
CB	16	13015.50			0.392		0	0.8	
CB	17	13039.31			0.408		0	1.5	
HB	37	13106.63	13842.93		0.40		−0.055	1.5	(0,1,0)
CB	18	13134.13			0.392		0	1.5	
CB	19	13146.29		7.74	0.415		0	0.6	
HB	39	13165.86	13902.10		0.37		0	1.5	(0,1,0)
CB	20	13231.60			0.393		0	1.5	
CB	21	13244.84		8.04	0.400	0.0002	0	2.7	
CB	22	13262.43			0.416		0.034	0.5	
HB	42	13296.80	14033.37		0.40		0	0.8	(0,1,0)
CB	23	13301.69		7.71	0.401	0.0000	0	1.2	
CB	24	13337.79			0.406	0.0001	0	1.1	
CB	25	13343.19			0.388		0	1.5	
CB	26	13353.28			0.394		−0.030	0.7	
CB	27	13385.58			0.400		0	0.5	
CB	28	13434.79			0.373		−0.199	1.9	
HB	49	13456.77	14193.18		0.39		0	1.5	(0,1,0)
HB	50	13492.64	14229.00		0.39		0	0.8	(0,1,0)
HB	51	13504.38	14240.72		0.38		0	1.5	(0,1,0)
CB	29	13519.06			0.458		0	1.5	
CB	30	13566.95			0.397		0	0.8	
	31	13649.81		6.54	0.389		0	0.8	
CB	32	13667.04			0.391		−0.034	0.5	
	33	13677.15			0.376		0	0.8	
	34	13719.90			0.400		0	0.8	
	35	13830.65			0.393		0	1.2	
CB	36	13842.93			0.406		−0.043	0.5	
	37	13889.64			0.407		−0.025	0.8	
CB	38	13902.10			0.388		0	0.5	
	39	13929.76			0.395		0	0.8	
	40	13975.39			0.392		0	0.8	
	41	14029.44			0.396		−0.008	1.5	
CB	42	14033.37			0.403		0	0.5	
	43	14039.05			0.401	0.0001	0	1.4	
	44	14058.69			0.389		0	1.5	
	45	14081.04			0.407		0	0.5	
	46	14120.84			0.383		0	0.8	
	47	14156.83		7.98	0.388		0	0.5	
CB	48	14193.18			0.395		0	0.8	
CB	49	14229.00			0.391		0	0.5	
CB	50	14240.72			0.385		0	0.8	
	51	14276.86			0.365		−0.101	1.9	
	52	14299.92			0.390		0	0.8	
	53	14313.87			0.389		0	2.6	

HB# indicates a hot band that corresponds to a cold band CB#.

corresponding hot bands have been observed at longer wavelengths. Using the ratio of hot and cold bands observed for the main isotopologue, we estimate that only (2 ± 1) of the 16 unassigned bands are hot bands. Globally, this gives (51 ± 1) cold bands and (10 ± 1) hot bands in the studied range.

A number of Q-branches have been observed that must be due to $K = 1$ sub-bands. Although no complete $K = 1$ sub-bands have been identified—presumably because of overlap—Q-branches of the $K = 1$ sub-band have been assigned for 15 vibronic bands. For these bands the value of the rotational A' constant has been estimated.

The band shown in Fig. 3 shows clear fine structure splitting for higher N-levels, but in most cases fine structure is not observed for this isotopologue. An overview with the constants of all observed bands for this isotopologue is given in Table 7.

4. Discussion

The majority of the results presented here is new. So far no electronically excited state constants have been derived for the $^{18}O^{14}N^{18}O$ and $^{18}O^{14}N^{16}O$ species and the bands presented here for $^{16}O^{14}N^{16}O$ have been fitted in an accurate way independently from results presented in earlier studies [11,18]. It is interesting at this stage to investigate whether the extensive data sets for both symmetric ($^{16}O^{14}N^{16}O$, $^{16}O^{15}N^{16}O$ [1] and $^{18}O^{14}N^{18}O$) and asymmetric $^{18}O^{14}N^{16}O$ isotopologues can be used to quantify the symmetry dependence of vibronic couplings. Such a dependence should be reflected in the molecular parameters.

Initially we hoped to find a clear relationship between values of the rotational constants and the degree of mixing of the electronic ground state and the first electronically excited state, but this relationship is far from obvious. Clearly most of the fitted bands result in $1/2(B' + C')$ constants that are close to or within 5% of the ground state value. This is illustrated for the four isotopologues in Fig. 4 where the distribution of the $1/2(B' + C')$ values is given. This distribution peaks around the value that corresponds to a common equilibrium geometry with appropriate change of masses. For the isotopologues studied here average values for $1/2(B' + C')$ of 0.420(27) cm^{-1} for $^{16}O^{14}N^{16}O$, 0.402(19) cm^{-1} for $^{18}O^{14}N^{16}O$ and 0.375(17) cm^{-1} for $^{18}O^{14}N^{18}O$ are derived in the studied energy range. In a limited number of particularly stronger bands, a substantial (>5%) increase of $1/2(B' + C')$ is observed and this indicates an upper level with strong A^2B_2 electronic character. In contrast, also a few $1/2(B' + C')$ values are found that are significantly smaller than the average; in these cases the bands turn out to have a weak intensity and the fitted constants should be regarded as effective parameters only.

A strong A^2B_2 electronic character can also be predicted for bands with substantially lower A-values (<7 cm^{-1}). These considerations, however, are clearly not sufficient to conclude on the degree of vibronic mixing between the ground and electronically excited state. This frustrates efforts to categorize excited states according to strong or weak vibronic couplings and to use such information for a vibrational assignment. However, additional information on the vibronic coupling strength and its symmetry dependence can be derived from the number of observed vibronic transitions, a comparison of relative intensities and the size of the fine structure splitting.

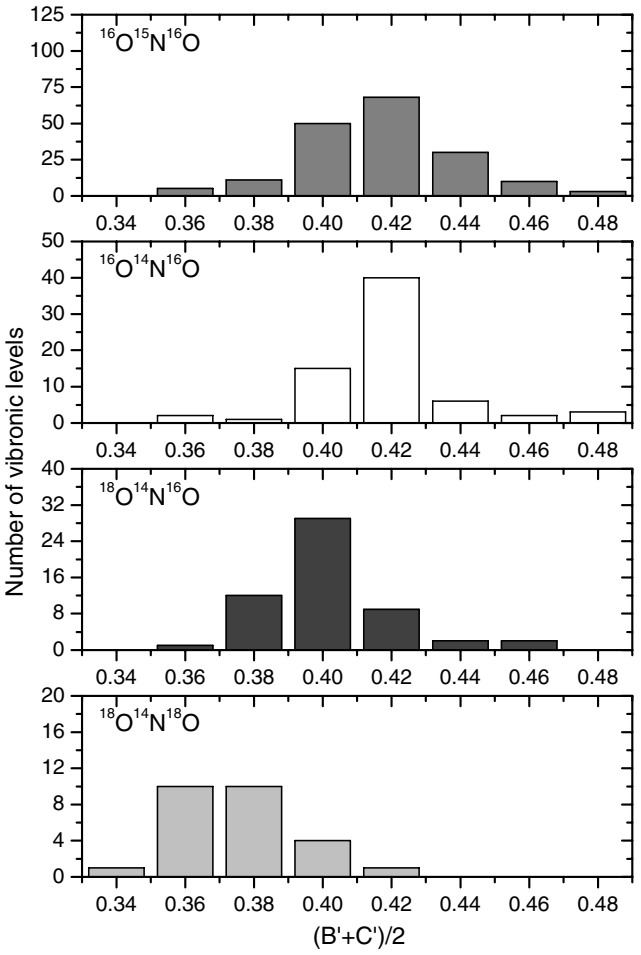

Fig. 4. Four histograms showing the distribution of $1/2(B' + C')$ values found for the electronically excited state as available from Ref. [1] for the symmetric $^{16}O^{15}N^{16}O$ and from this work for both the symmetric $^{16}O^{14}N^{16}O$ and $^{18}O^{14}N^{18}O$ (Tables 3 and 5) and asymmetric $^{18}O^{14}N^{16}O$ species (Table 7). Note that the energy range studied in Ref. [1] and in the present work are different.

The investigated energy range is relatively close to the conical intersection which is located just below 10000 cm^{-1}, and this is indeed reflected in an overall spectrum that is substantially less dense than observed for higher energies. For an asymmetric NO_2 isotopologue one expects a vibronic density approximately twice as large as for a symmetric isotopologue because of the merging of B_2 and A_1 species (in C_{2v} symmetry) into a single A' species (in C_s symmetry). This is roughly confirmed in the present study by the ratio of the number of observed cold bands for $^{18}O^{14}N^{16}O$ and $^{18}O^{14}N^{18}O$—51 to 25—that is close to 2. However, the numbers of $^{16}O^{14}N^{16}O$ and $^{18}O^{14}N^{18}O$ cold

Table 8
Overview of bands with effective constants (cm^{-1}) that cannot be assigned to a regular band of one of the isotopologues studied here

Origin	$1/2(B''+C'')$	$1/2(B'+C')$	$1/2(\varepsilon'_{22}+\varepsilon'_{33})$	$\Delta(1/2(B'+C'))\times 10^3$	Symmetry
12379.31	0.311	0.327	0	1.4	C_{2v}
12775.30	0.294	0.298	0	0.3	C_s
12818.45	0.315	0.324	−0.12	0.5	C_{2v}
12878.53	0.315	0.316	0	0.6	C_{2v}
12903.78	0.316	0.324	−0.11	0.2	C_{2v}

bands should be about the same in the studied energy range for the used mixture and this is clearly not the case. This discrepancy is not fully understood and may be due to an oxygen isotope exchange process between NO_2 and other compounds in favor of ^{16}O containing isotopologues. A detailed study of the relative intensities of the various vibronic bands of the three isotoplogues should allow to understand this discrepancy. Unfortunately, fast degrading infrared dyes prohibit a direct measurement of relative intensities. This experimental limitation can be countered by using previously recorded $^{16}O^{14}N^{16}O$ data [11,20] as a set of reference intensities to normalize the present results. This analysis is outside the scope of the present work.

In addition, a global weakening of the fine structure splittings of vibronic bands of C_s geometry has been observed: the value of the average fine structure splitting of $^{18}O^{14}N^{16}O$ is about a factor 10 smaller than for $^{16}O^{14}N^{16}O$. Work is currently in progress to relate the intensity pattern and the size of the fine structure splitting to symmetry dependent vibronic coupling strengths. This will be topic of a separate paper [32].

Acknowledgments

The Netherlands Organization for Scientific Research (NWO), the Dutch organization for Fundamental Research (FOM) through the MAP program, the Netherlands Research School for Astronomy are acknowledged for financial support. We thank Drs. Harald Verbraak for his help in characterizing the $^xO^yN^zO$ mixture and Drs. Arno Vredenborg for his help in the initial stage of this work. R.J., who belongs to ENSPG-INP Grenoble, acknowledges EU support for several visits to the Laser Center Vrije Universiteit within the integrating infrastructure initiative: contract RII3-CT-2003-506350.

Appendix A. APPENDIX—unidentified bands

In total 173 bands have been identified and assigned to one of the three isotopologues studied in this work. In the frequency region of 11 800–14 380 cm^{-1} five more bands have been observed that have not been identified. These bands are very comparable to the C_s and C_{2v} spectra shown in Figs. 1–3, but the rotational ground state constants that have to be used to reproduce the observed transitions are far from any value listed in Table 1. The list with bands and derived constants is listed for completeness in Table 8.

References

[1] E.A. Volkers, M.C. Koudijzer, A. Vredenborg, J. Bulthuis, S. Stolte, H. Linnartz, R. Jost, J. Mol. Spectrosc. 235 (2006) 1–17.
[2] R. Jost, G. Michalski, M. Thiemens, J. Chem. Phys. 123 (2005) 054320 (1–10).
[3] G. Michalski, R. Jost, D. Sugny, M. Joyeux, M. Thiemens, J. Chem. Phys. 121 (2004) 7153–7161.
[4] M. Joyeux, R. Jost, M. Lombardi, J. Chem. Phys. 119 (2003) 5923–5932.
[5] R. Jost, M. Garcia Vergniory, A. Campargue, J. Chem. Phys. 119 (2003) 2590–2595.
[6] V. Kurkal, P. Fleurat-Lessard, R. Schinke, J. Chem. Phys. 119 (2003) 1489–1501.
[7] S. Heilliette, A. Delon, D. Reignier, T. Stoecklin, J.C. Rayez, Phys. Chem. Chem. Phys. 5 (2003) 2039–2046.
[8] R. Jost, M. Joyeux, M. Jacon, Chem. Phys. 283 (2002) 17–28.
[9] A. Delon, R. Jost, M. Jacon, J. Chem. Phys. 114 (2001) 331–344.
[10] C.A. Biesheuvel, J. Bulthuis, M.H.M. Janssen, S. Stolte, J.G. Snijders, J. Chem. Phys. 112 (2000) 3633–3642.
[11] A. Delon, R. Jost, J. Chem. Phys. 110 (1999) 4300–4308.
[12] C.A. Biesheuvel, J. Bulthuis, M.H.M. Janssen, J.G. Snijders, S. Stolte, J. Chem. Phys. 109 (1998) 9701–9712.
[13] J. Orphal, S. Dreher, S. Voigt, J.P. Burrows, R. Jost, A. Delon, J. Chem. Phys. 109 (1998) 10217–10221.
[14] J. Liévin, A. Delon, R. Jost, J. Chem. Phys. 108 (1998) 8931–8943.
[15] B. Kirmse, A. Delon, R. Jost, J. Chem. Phys. 108 (1998) 6638–6651.
[16] A. Delon, R. Georges, B. Kirmse, R. Jost, Faraday Discuss. 102 (1995) 117–128.
[17] A. Delon, R. Georges, R. Jost, J. Chem. Phys. 103 (1995) 7740–7772.
[18] R. Georges, A. Delon, F. Bylicki, R. Jost, A. Campargue, A. Charvat, M. Chenevier, F. Stoeckel, Chem. Phys. 190 (1995) 207–229.
[19] D. Romanini, P. Dupre, R. Jost, Vib. Spectrosc. 19 (1999) 93–106.
[20] R. Georges, A. Delon, R. Jost, J. Chem. Phys. 103 (1995) 1732–1747.
[21] E.A. Volkers, A. Vredenborg, H. Linnartz, J. Bulthuis, S. Stolte, R. Jost, Chem. Phys. Lett. 391 (2004) 106–111.
[22] H. Linnartz, D. Verdes, T. Speck, Rev. Sci. Instrum. 71 (2000) 1811–1815.
[23] H. Verbraak, J.N.P. van Stralen, J. Bouwman, J.S. de Klerk, D. Verdes, H. Linnartz, F.M. Bickelhaupt, J. Chem. Phys. 123 (2005) 144305 (1–8).
[24] W.C. Bowman, F.C. de Lucia, J. Chem. Phys. 77 (1982) 92–107.
[25] A. Perrin, C. Camy-Peyret, J.-M. Flaud, J. Mol. Spectrosc. 130 (1988) 168–182.
[26] A. Perrin, J.-M. Flaud, C. Camy-Peyret, A. Goldman, F.J. Murcray, R.D. Blatherwick, C.P. Rinsland, J. Mol. Spectrosc. 160 (1993) 456–463.
[27] G.R. Bird, J.C. Baird, A.W. Jache, J.A. Hodgeson, R.F. Curl Jr., A.C. Kunkle, J.W. Bransford, J. Rastrup-Andersen, J. Rosenthal, J. Chem. Phys. 40 (1964) 3378–3390.
[28] J.L. Hardwick, J.C.D. Brand, Can. J. Phys. 54 (1976) 80–91.
[29] J.C.D. Brand, J.L. Hardwick, K.E. Teo, Can. J. Phys. 54 (1976) 1069–1076.
[30] C.H. Townes, A.L. Schawlow, Microwave Spectroscopy, Dover Publications, USA, 1975.
[31] H.J. Vedder, M. Schwartz, H.-J. Foth, W. Demtröder, J. Mol. Spectrosc. 97 (1983) 92–116.
[32] E.A. Volkers et al. (in preparation).